Electronic Supplementary Material (ESI) for Journal of Materials Chemistry C.


# Supporting information to: Computational prediction and characterization of CuI-based ternary $p$-type transparent conductors

Michael Seifert* and Tomáš Rauch†
*Institut für Festkörpertheorie und -optik, Friedrich-Schiller-Universität Jena, Max-Wien-Platz 1, 07743 Jena, Germany and European Theoretical Spectroscopy Facility*

Miguel A. L. Marques‡
*Research Center Future Energy Materials and Systems of the Research Alliance Ruhr Faculty of Mechanical Faculty of Mechanical Engineering and ICAMS, Ruhr University Bochum, Universitätstrasse 150, 44780 Bochum, Germany and European Theoretical Spectroscopy Facility and European Theoretical Spectroscopy Facility*

Silvana Botti§
*Institut für Festkörpertheorie und -optik, Friedrich-Schiller-Universität Jena, Max-Wien-Platz 1, 07743 Jena, Germany and European Theoretical Spectroscopy Facility Research Center Future Energy Materials and Systems of the Research Alliance Ruhr Faculty of Physics and ICAMS, Ruhr University Bochum, Universitätstrasse 150, 44780 Bochum, Germany*
(Dated: April 22, 2024)

## I. DEFINITION OF $p$-TYPE DEGENERATE SEMICONDUCTOR

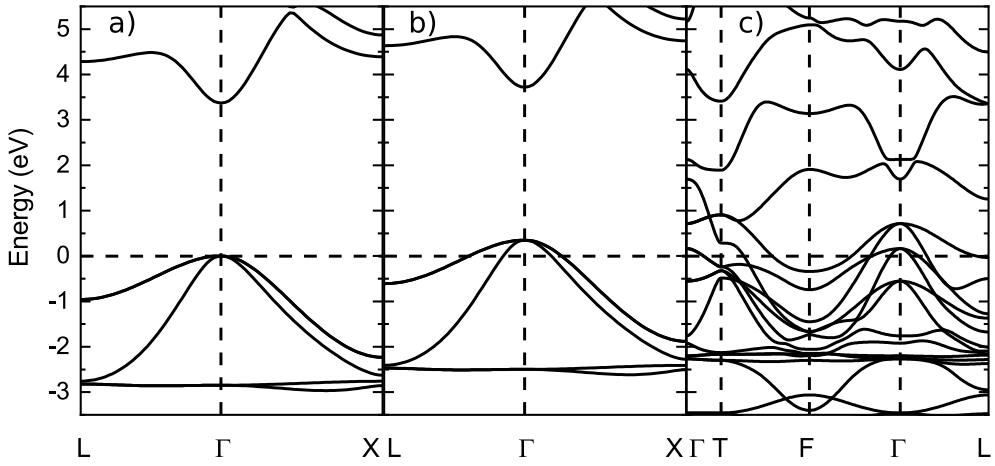


FIG. S1. Representative band structures of (a) a semiconductor, (b) a p-type degenerate semiconductor and (c) a metal.

In Fig. S1 representative band structures of a) a semiconductor, b) a p-type degenerate semiconductor and c) a metal are shown. In the case of a semiconductor, the Fermi level is located inside the band gap, inducing transparency of the material up to the energy of the minimum band gap (neglecting excitonic effects). The Fermi level of a metal crosses one or more bands and no energy gap is present in the band structure close to it. As a result, the metal absorbs light in the visible range of the light spectrum. In the case of the p-type degenerate semiconductor, the Fermi level is located below the valence band maximum, but a band gap still separates the occupied and empty bands. This results in absorption in the infrared due to transitions between occupied and empty states in the valence band, an absorption gap corresponding to the band gap, and then absorption at higher energies due to transitions between valence and conduction bands. If the distance between the Fermi level and the valence band maximum is small enough, transparency in the visible range of frequencies can be realised.

* michael.seifert@uni-jena.de
† tomas.rauch@uni-jena.de
‡ miguel.marques@rub.de
§ silvana.botti@uni-jena.de

## II. LIST OF STOICHIOMETRIES CONSIDERED FOR THE MHM RUNS

TABLE S1. List of all stoichiometries considered for the MHM runs, together with the space group, the formation energy $E_{\text{for}}$ and the distance of the convex hull $\Delta E_{\text{hull}}$, obtained with PBE and SCAN, of the most stable structure found for each stoichiometry

| Composition | SG | $E_{\text{for}}^{\text{PBE}}$ (meV/at) | $\Delta E_{\text{hull}}^{\text{PBE}}$ (meV/at) | $\Delta E_{\text{hull}}^{\text{SCAN}}$ (meV/at) |
|---|---|---|---|---|
| $Cu_2S_2I$ | 187 | -143 | 18 | 37 |
| $CuS_2I$ | 14 | -118 | 0 | 23 |
| $CuS_2I_2$ | 8 | -30 | 65 | 95 |
| $CuS_3I$ | 1 | -30 | 65 | 79 |
| $Cu_2SI$ | 115 | -180 | 4 | 11 |
| $Cu_2SI_2$ | 1 | -84 | 64 | 104 |
| $Cu_3SI$ | 8 | -111 | 41 | 62 |
| $Cu_3SI_2$ | 44 | -179 | 0 | 4 |
| CuSI | 8 | -1 | 134 | 163 |
| $CuSI_2$ | 8 | -25 | 76 | 109 |
| $CuSI_3$ | 6 | -10 | 71 | 102 |
| $CuSI_4$ | 8 | 1 | 68 | 126 |
| $Cu_2Se_2I$ | 166 | -125 | 12 | 0 |
| $CuSe_2I$ | 14 | -132 | 0 | 0 |
| $CuSe_2I_2$ | 8 | -57 | 56 | 71 |
| $CuSe_2I_5$ | 1 | -50 | 31 | 69 |
| $CuSe_3I$ | 166 | -94 | 12 | 0 |
| $Cu_2SeI$ | 115 | -137 | 9 | 11 |
| $Cu_2SeI_2$ | 5 | -98 | 46 | 75 |
| $Cu_2SeI_4$ | 8 | -85 | 24 | 38 |
| $Cu_3SeI$ | 8 | -100 | 25 | 35 |
| CuSeI | 8 | -20 | 142 | 99 |
| $CuSeI_2$ | 8 | -26 | 86 | 56 |
| $CuSeI_3$ | 1 | -63 | 31 | 50 |
| $CuSeI_4$ | 8 | -48 | 43 | 54 |
| $Cu_3SeI_2$ | 8 | -152 | 0 | 1 |

## III. CRYSTAL STRUCTURES OF STABLE TERNARY COMPOUNDS

Here we show pictures of the crystal structures discussed in the manuscript. In Fig. S2 (a,c,e) the structures of group 1) zincblende-type ordered alloys are shown, in Fig. S2 (b,d) the structures of group 3) indirect semiconductors with chalcogen-chalcogen bonds, and in Fig. S3 the miscellaneous structures of group 4). The structures of group 2) topological semimetals are already shown in Fig. 4 of the main manuscript.

Regarding $Cu_2SeI_4$, it is noteworthy the formation of triiodide ($I_3^-$) with an angle of 175.2° and a longer (3.57 Å) and shorter (3.20 Å) I-I bond. These results are similar to triiodide formations within other host materials [2]. Furthermore, it was discussed, that a I interstitial next to a Cu vacancy in $\gamma$-CuI will also lead to triiodide [3].

## IV. ADDITIONAL BAND STRUCTURES

In Fig. S4 a) we plot the band structure of CuI computed using HSE06 with an adjusted $\alpha$=0.32 (black) together with the band structure calculated with PBE0. The value of $\alpha$ was chosen to reproduce the experimental band gap of 3.1 eV. We do not include spin-orbit coupling in these calculations, and we can therefore observe that the PBE0 band gap is slightly larger than 3.1 eV. Nevertheless, we observe that the band dispersions are very similar.

In Fig. S4 b) and Fig. S5 the remaining band structures from the manuscript are shown calculated with HSE06 using the modified $\alpha = 0.32$. We see in Fig. S5 a) that $Cu_2SeI_4$ is a $p$-type degenerate semiconductor, but it was not included as a potential structure for $p$-type TCM since the optical gap is too small.

In Fig. S6 we show the band structures of $Cu_2S_2I$ and $Cu_2Se_2I$, calculated with different exchange-correlation functionals to accompany the discussion of those materials in the manuscript.

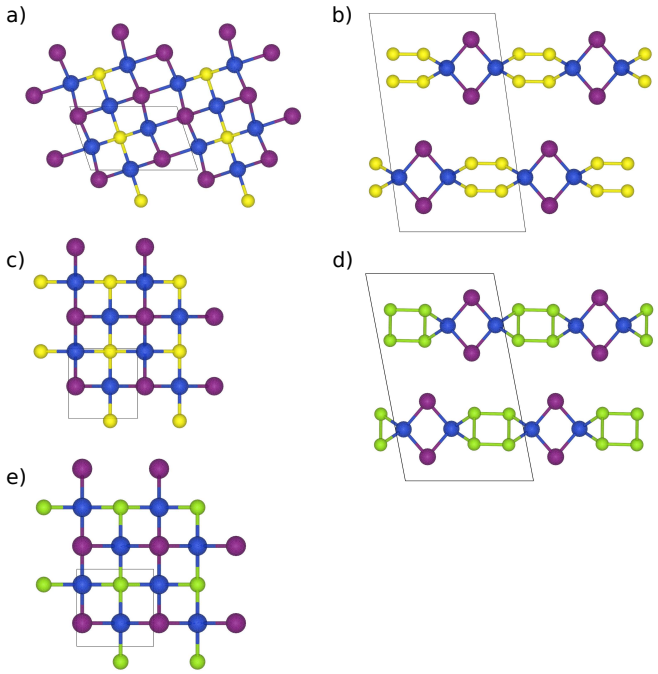


FIG. S2. Crystal structures of zincblende-type ordered alloys: a) $Cu_3SI_2$, c) $Cu_2SI$, e) $Cu_2SeI$. Crystal structures of indirect semiconductors with chalcogen-chalcogen bonds: b) $CuS_2I$, d) $CuSe_2I$. The images were produced using VESTA [1]. Blue balls represent Cu, violet I, yellow S and green Se atoms. The unit cells are marked by black lines.

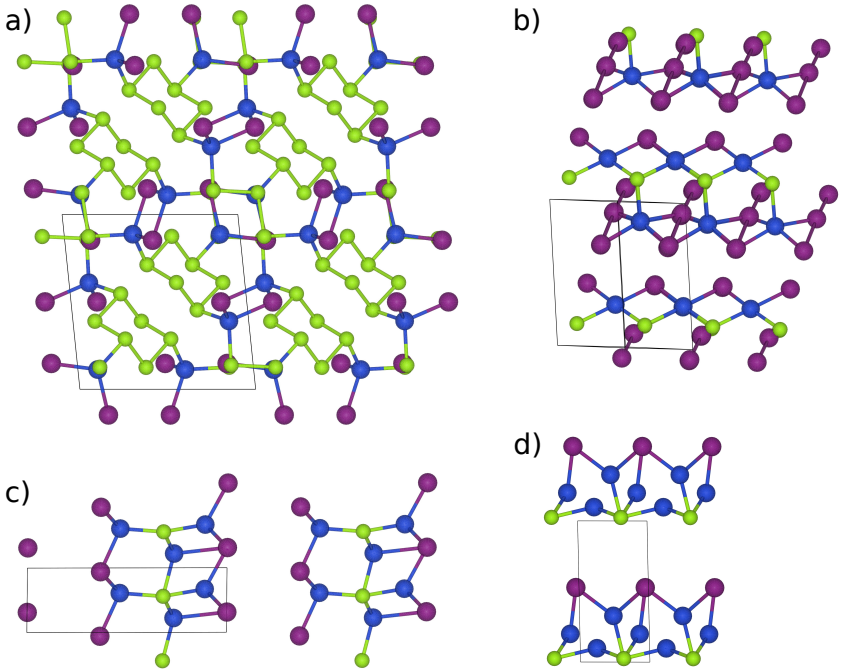


FIG. S3. Crystal structures of miscellaneous compounds: a) $CuS3_3I$, b) $Cu_2SeI_4$, c) $Cu_3SeI_2$ and d) $Cu_3SeI$. The images were produced using VESTA [1]. Blue balls represent Cu, violet I, yellow S and green Se atoms. The unit cells are marked by the black lines.

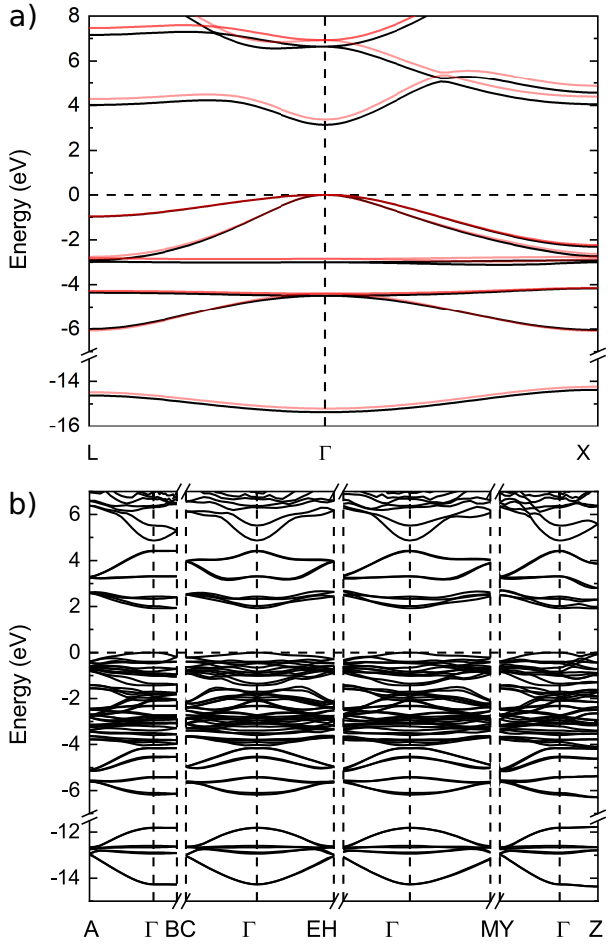


FIG. S4. a) Band structure of CuI calculated with HSE06 with adjusted $\alpha$=0.32 (black) and PBE0 (red), b) band structures $CuSe_2I$ calculated with HSE06 with adjusted $\alpha$=0.32.

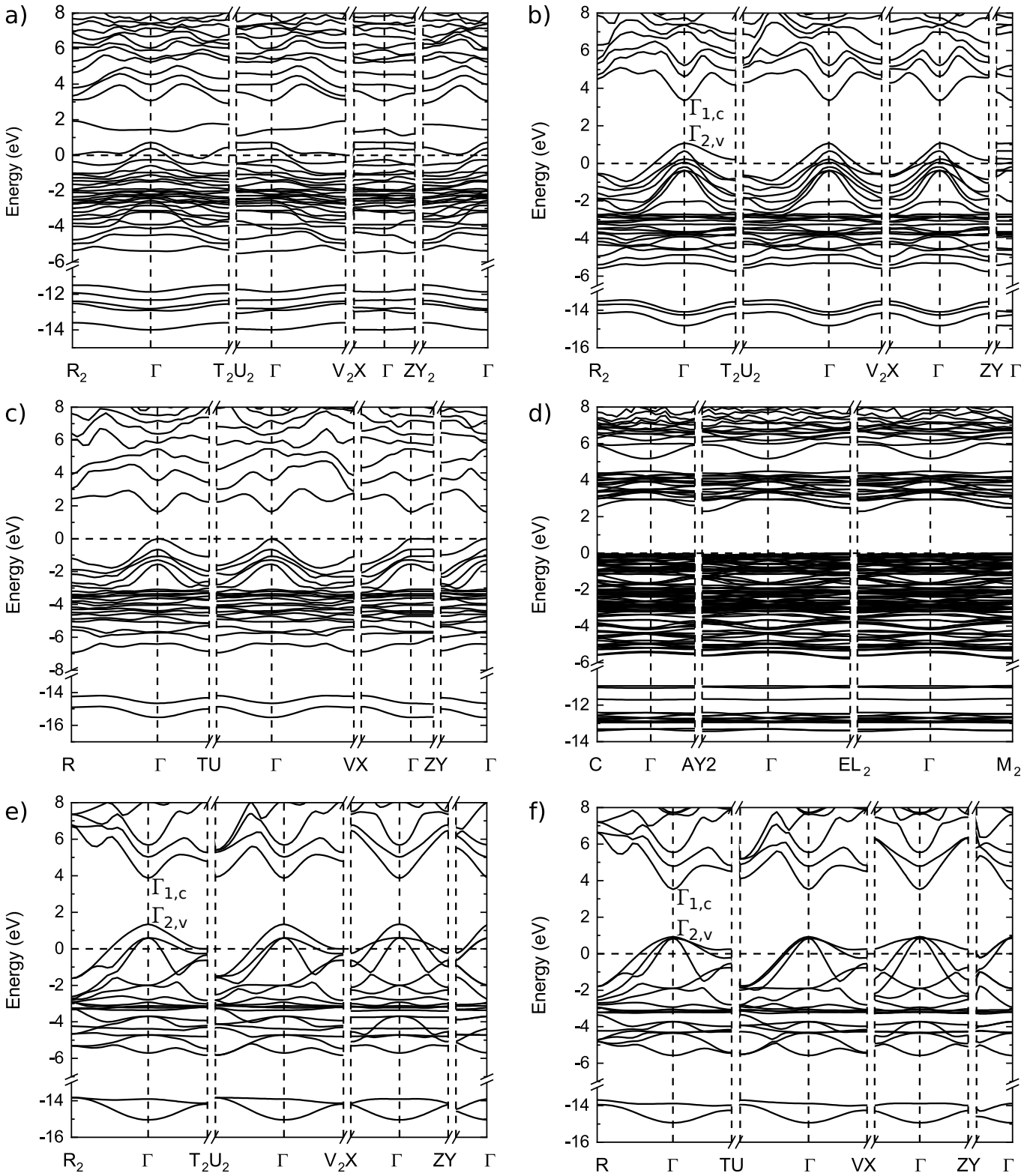


FIG. S5. Band structures of a) $Cu_2SeI_4$, b) $Cu_3SeI_2$, c) $Cu_3SeI$, d) $CuSe_3I$, e) $Cu_2SI$ and f) $Cu_2SeI$ calculated with HSE06 and adjusted $\alpha = 0.32$.

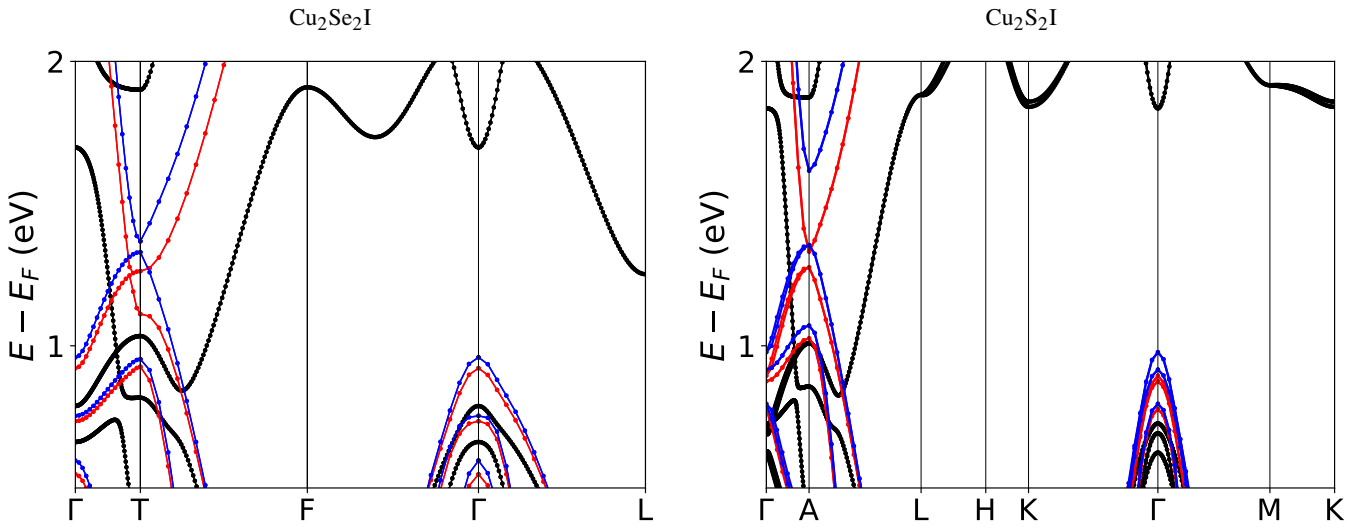


FIG. S6. Band structures of $Cu_2Se_2I$ (left) and $Cu_2S_2I$ (right) calculated with PBE (black), HSE06 (red), and HSE06 with modified $\alpha = 0.32$ (blue). Spin-orbit coupling was included in all calculations.

## V. ADDITIONAL EFFECTIVE MASSES

TABLE S2. Effective masses in additional directions with respect to those listed in Table 4 of the main manuscript. We consider only structures discussed as possible p-type TCM.

| Composition | PBE $m^h_{\text{eff}}$ | direction | PBE $m^h_{\text{eff}}$ | direction | PBE $m^h_{\text{eff}}$ | direction | PBE $m^h_{\text{eff}}$ | direction | PBE $m^h_{\text{eff}}$ | direction |
|---|---|---|---|---|---|---|---|---|---|---|
| $Cu_3SI_2$ | 0.54 | $\Gamma \rightarrow R_2$ | 0.97 | $\Gamma \rightarrow T_2$ | 0.49 | $\Gamma \rightarrow U_2$ | 0.28 | $\Gamma \rightarrow X$ | 0.97 | $\Gamma \rightarrow Z$ |
| $Cu_2SI$ | 0.58 | $\Gamma \rightarrow R$ | 0.88 | $\Gamma \rightarrow U$ | 0.47 | $\Gamma \rightarrow V$ | 0.70 | $\Gamma \rightarrow X$ | 0.88 | $\Gamma \rightarrow Z$ |
| $Cu_3SeI_2$ | 0.52 | $\Gamma \rightarrow R_2$ | 1.28 | $\Gamma \rightarrow T_2$ | 0.52 | $\Gamma \rightarrow U_2$ | 0.26 | $\Gamma \rightarrow V_2$ | 1.31 | $\Gamma \rightarrow Z$ |
| $Cu_2SeI$ | 0.45 | $\Gamma \rightarrow R$ | 0.68 | $\Gamma \rightarrow U$ | 0.36 | $\Gamma \rightarrow V$ | 0.69 | $\Gamma \rightarrow X$ | 0.69 | $\Gamma \rightarrow Z$ |
| CuI | 0.21 | $\Gamma \rightarrow X$ | 0.20 | $\Gamma \rightarrow L$ | | | | | | |

[1] K. Momma and F. Izumi, J. Appl. Crystallogr. **44**, 1272 (2011).
[2] K.-F. Tebbe and U. Georgy, Acta Crystallographica Section C **42**, 1675 (1986).
[3] S. Koyasu, N. Umezawa, A. Yamaguchi, and M. Miyauchi, J. Appl. Phys. **125**, 115101 (2019), https://doi.org/10.1063/1.5082865.